Research on Dead Reckoning Algorithm for Self-Propelled Pipeline Robots in Three-Dimensional Complex Pipelines

Yan Gao[1]
School of Mechanics and Engineering Science
Peking University
Beijing, China
gloriagaohu@stu.pku.edu.cn

Jiliang Wang[1]
School of Advanced Manufacturing and Robotics
Peking University
Beijing, China
wangjiliang@pku.edu.cn

Minghan Wang
School of Mechanics and Engineering Science
Peking University
Beijing, China
wangminghan@stu.pku.edu.cn

Xiaohua Chen
School of Mechanics and Engineering Science
Peking University
Beijing, China
xiaohuachen25@stu.pku.edu.cn

Demin Chen
School of Mechanics and Engineering Science
Peking University
Beijing, China
chendemin_vip@pku.edu.cn

Zhiyong Ren
School of Mechanics and Engineering Science
Peking University
Beijing, China
renzhiyong@pku.edu.cn

Tian-Yun Huang*
School of Advanced Manufacturing and Robotics
Peking University
Beijing, China
huangtianyun@pku.edu.cn

***Abstract*—In the field of gas pipeline location, existing pipeline location methods mostly rely on pipeline location instruments. However, when faced with complex and curved pipeline scenarios, these methods often fail due to problems such as cable entanglement and insufficient equipment flexibility. To address this pain point, we designed a self-propelled pipeline robot. This robot can autonomously complete the location work of complex and curved pipelines in complex pipe networks without external dragging. In terms of pipeline mapping technology, traditional visual mapping and laser mapping methods are easily affected by lighting conditions and insufficient features in the confined space of pipelines, resulting in mapping drift and divergence problems. In contrast, the pipeline location method that integrates inertial navigation and wheel odometers is less affected by pipeline environmental factors. Based on this, this paper proposes a pipeline robot location method based on extended Kalman filtering (EKF). Firstly, the body attitude angle is initially obtained through an inertial measurement unit (IMU). Then, the extended Kalman filtering algorithm is used to improve the accuracy of attitude angle estimation. Finally, high-precision pipeline location is achieved by combining wheel odometers. During the testing phase, the roll wheels of the pipeline robot needed to fit tightly against the pipe wall to reduce slippage. However, excessive tightness would reduce the flexibility of motion control due to excessive friction. Therefore, a balance needed to be struck between the robot's motion capability and positioning accuracy. Experiments were conducted using the self-propelled pipeline robot in a rectangular loop pipeline, and the results verified the effectiveness of the proposed dead reckoning algorithm.**

Keywords—Pipeline robots, Self-propelled, Complex pipeline localization, Dead reckoning

I. INTRODUCTION

With the advancement of urbanization, the scale of urban underground pipe networks is rapidly expanding. As a core facility for energy supply, the safety inspection of gas pipelines is becoming increasingly important. Obtaining the three-dimensional location coordinates of pipelines is the key to leak prevention and efficient inspection, and it is also a current research hotspot [1]. The existing mainstream methods for external positioning of gas pipelines have formed a diverse technical system, mainly including ground-penetrating radar [2], acoustic detection positioning [3], magnetic gradient positioning [4], and fiber optic sensing positioning [5]. These pipeline positioning methods exhibit different adaptability and accuracy performance in different pipeline positioning scenarios.

Regarding the internal positioning of gas pipelines, currently, visual SLAM [6], laser SLAM [7], or multi-sensor fusion schemes are commonly used for 3D positioning and mapping [8]. However, the dim lighting, sparse texture, and insufficient feature points inside the pipeline make it easy for existing visual SLAM and laser SLAM technologies to diverge in the pipeline environment. In study [9], the pipeline locator based on Micro-Electro-Mechanical Systems (MEMS) IMU and wheel odometer can solve the problem of internal pipeline positioning to a certain extent, but the device has a core limitation. On the one hand, it relies on external cable dragging to achieve drive, and on the other hand, it cannot autonomously plan the movement path. Therefore, its applicability is significantly reduced when dealing with complex pipeline network structures, especially when facing elbows, T-branches, tapering pipes and sloped pipes. Not only are the cables easily tangled and hinder the movement, but the inability to autonomously adjust the direction of travel and the difficulty in adapting to different pipe diameters also limit the positioning range and flexibility. In study [10], some researchers have used a pipeline robot to drag an inertial navigation positioning module to achieve three-dimensional positioning of complex pipeline networks. However, this solution requires an additional inertial navigation module to be dragged to the tail of the robot and relies on external cables for power. The cable entanglement problem

means that the robot can only complete short-distance positioning and detection. Most of the existing pipeline robots with high passing ability mostly rely on cables for external power supply, and the length of the cables limits the maximum inspection mileage [11], [12], [13], [14].

Considering the aforementioned challenges, we have designed a self-propelled cable-free pipeline robot. The robot is integrated with inertial navigation, equipped with a wireless remote control system, and furnished with a built-in power supply module. What's more, the robot can smoothly pass through various complex pipelines and autonomously choose pipeline paths in complex pipe networks, meeting the three-dimensional positioning requirements of multi branch pipe networks. In order to avoid environmental interference in the precise positioning of pipelines, we use the dead reckoning algorithm to recursively calculate the robot's attitude changes to achieve pipeline positioning [15], [16]. Although this method is independent of external environmental signals, it is affected by accumulated sensor errors [17]. Therefore, this article proposes an improved dead reckoning algorithm that integrates inertial navigation and wheel odometry into a self-propelled pipeline robot, achieving precise positioning in complex pipeline networks.

The remainder of this paper can be organized as follows. First, Section II elaborates on the design and research of the self-propelled pipeline robot. Then, Section III details the dead reckoning algorithm of the pipeline robot. Next, Section IV presents the experimental verification and result analysis of the proposed method. Finally, a concluding discussion is provided in Section V.

II. Self-propelled Pipeline Robot Design

A. Composition Structure of Self-Propelled Pipeline Robot

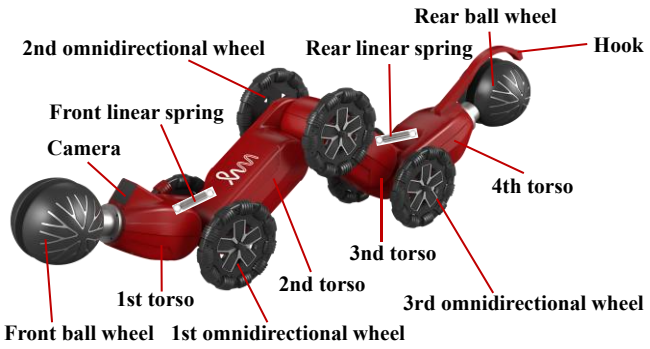

Fig. 1. Schematic diagram of self-propelled pipeline robot structure.

As depicted in Fig. 1, we designed and developed a self-propelled wireless pipeline-handling robot for natural gas pipeline positioning and inspection. The body of the self-propelled pipeline robot consists of four torso sections, each with a battery and motor inside. The motors inside the second and third torso sections are driven by bevel gear transmission to drive three pairs of omnidirectional wheels to rotate, and the front and rear roll wheels are directly driven to rotate by the motors. Between the first and second sections, and between the third and fourth sections, there is a direct tension spring connection. The robot's head is equipped with a camera and LED light strip, which can conduct inspections inside the pipeline. The tail is equipped with a hook, which can drag heavy objects. Due to the modular installation of pipeline robots, the camera and hook modules can be adjusted and installed as needed.

B. Hardware and Signal Transmission Scheme of Self-propelled Pipeline Robot

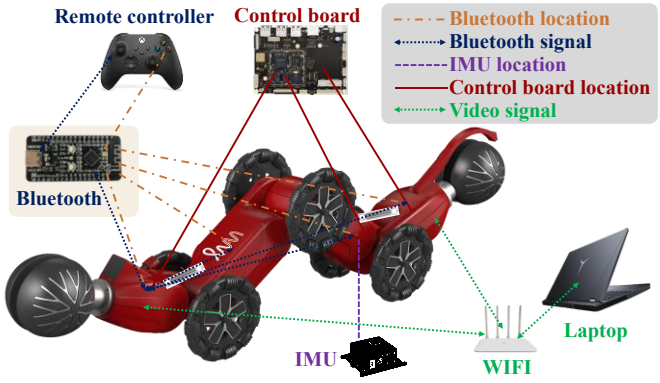

Fig. 2. Schematic diagram of wireless communication data transmission method for pipeline robots.

Fig. 2 shows the hardware signal transmission and communication scheme for the self-propelled pipeline robot. Our pipeline robot is designed with each modular body section housing a planetary geared motor, motor drive board, wireless communication module, main control board, and power supply module. Each body module can independently achieve wireless drive control. In addition, to achieve pipeline positioning, we installed a high-precision MEMS IMU on the third torso section of the pipeline robot. The main control boards in the first and last body sections are used for visual signal processing, while the control chip in the third body section is responsible for high-precision IMU signal acquisition and transmission.

To meet the needs of pipelines with varying inspection lengths, we designed three differentiated wireless communication strategies. For short-range communication (approximately 30 m), Bluetooth is used, ensuring low power consumption and effectively improving the overall battery life. During Bluetooth communication, the first body section acts as the Bluetooth master, while the remaining body sections act as slaves. The remote controller first communicates with the master, which then distributes commands to the other body sections. For medium-range communication (approximately 100 m), a combination of Wi-Fi and Bluetooth is used. Small data control signals are transmitted wirelessly via Bluetooth, while large video data is prioritized for transmission to the user's computer via Wi-Fi. This enables wireless Closed-Circuit Television (CCTV) pipeline inspection, allowing simultaneous operation of the pipeline robot and observation of the surrounding environment. When the Wi-Fi signal is weak, video data can be automatically recorded to a memory card for subsequent offline analysis. To ensure long-range wireless communication (approximately 1 km), a LoRa wireless communication method with a frequency of 433 MHz is required. While this communication scheme cannot transmit large data volumes such as video, and can only transmit simple motion control commands, it ensures the reliability of the robot's operation.

The performance parameters of the self-propelled pipeline robot designed in this study are listed in Table I. The robot measures 0.82 m in length, 0.15 m in width, and 0.28 m in height, with a total mass of 10.04 kg. In terms of endurance, it can operate continuously for up to 2 hours, covering a maximum range of 1000 m, which meets the inspection requirements of most medium-length pipelines. For wireless communication, different protocols can be selected based on the actual pipeline operation scenario, ensuring stable signal transmission between the robot and external control devices. Regarding load capacity, the robot exhibits varying traction capabilities for pipelines of different diameters: it can generate a traction force of 130 N for a 200-mm-diameter pipe and 60 N for a 250-mm-diameter pipe, demonstrating strong load-bearing performance and satisfying the needs for towing heavy objects and mounting inspection equipment.

TABLE I. PARAMETERS OF SELF-PROPELLED PIPELINE ROBOT

Parameter Names	Units	Values
Length	m	0.82
Width	m	0.15
Height	m	0.28
Mass	kg	10.04
Maximum Endurance Working Time	h	2
Maximum Endurance Range	m	1000
Wireless Communication Distance	m	1000
Dragging Ability (200 mm-diameter pipe)	N	130
Dragging Ability (250 mm-diameter pipe)	N	60

III. DEAD RECKONING ALGORITHM FOR PIPELINE ROBOTS

A. Establishment of Positioning Frame for Pipeline Robot

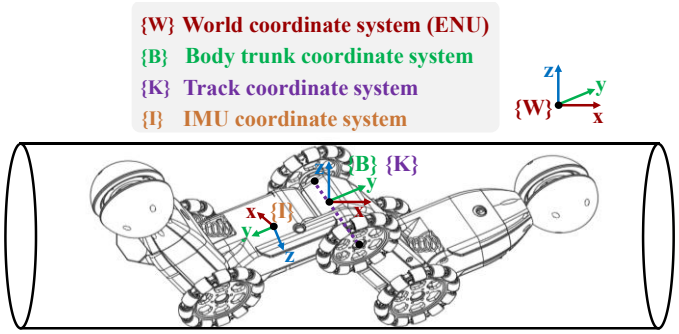

Fig. 3. Four key frames for pipeline robot positioning are defined as follows. The world frame {W} is the fixed global reference used to define the position and direction of the pipeline robot in the global frame. The body torso frame {B} is the local frame describing the robot's motion relative to itself. {N} is the navigation system used to describe the local motion of pipeline robots relative to the start point. The inertial navigation frame {I} is used for IMU measurement of the angular velocity and acceleration of the pipeline robot's body.

Fig. 3 indicates that the inertial module is installed in the third section of the pipeline robot body, and The orientation of each axis in the IMU frame {I} is determined by the position and orientation of the IMU installed on the pipeline robot. The defined navigation frame {N} is a local frame, with its origin at the center point of the middle roller wheel shaft of the pipeline robot at the initial moment. The forward direction of the pipeline robot is the x-axis, the direction opposite to gravity is the z-axis, and the y-axis is determined by the right-hand rule, pointing to the left side of the robot body. The origin of the body frame {B} is the center point of the middle roller shaft of the pipeline robot; the forward direction of the pipeline robot is the x-axis, the left side of the forward direction is the y-axis, and the z-axis is determined by the right-hand rule, generally pointing upward. The world frame {W} adopts the East-North-Up (ENU) frame.

The body acceleration measured in the navigation frame {N} is denoted as ${}^{\mathrm{N}}\mathbf{a}_{\mathrm{body}}$. When the pipeline robot is at its initial static state, ${}^{\mathrm{N}}\mathbf{a}_{\mathrm{body}}$ is equal to $\begin{bmatrix}0 & 0 & -\mathrm{g}\end{bmatrix}^{\mathrm{T}}$. The body acceleration measured in the IMU frame {I} is defined as ${}^{\mathrm{I}}\mathbf{a}_{\mathrm{body}}$, and the measured angular velocity is denoted as ${}^{\mathrm{I}}\boldsymbol{\omega}_{\mathrm{body}}$. The transformation relationship between the two frames is given by:

$$\begin{cases} {}^{\mathrm{N}}\mathbf{a}_{\mathrm{body}} = {}^{\mathrm{N}}\mathbf{R}_{\mathrm{I}} \cdot {}^{\mathrm{I}}\mathbf{a}_{\mathrm{body}} \\ {}^{\mathrm{N}}\boldsymbol{\omega}_{\mathrm{body}} = {}^{\mathrm{N}}\mathbf{R}_{\mathrm{I}} \cdot {}^{\mathrm{I}}\boldsymbol{\omega}_{\mathrm{body}} \end{cases} \tag{1}$$

where, ${}^{\mathrm{N}}\mathbf{R}_{\mathrm{I}} \in \mathbb{R}^{3\times3}$ is the rotation matrix converted from the IMU frame {I} to the navigation frame {N}, which can be measured at the initial stationary moment of the pipeline robot. The conversion relationship from the inertial frame {I} to the body frame {B} is:

$$\begin{cases} {}^{\mathrm{B}}\mathbf{a}_{\mathrm{body}} = {}^{\mathrm{B}}\mathbf{R}_{\mathrm{I}} \cdot {}^{\mathrm{I}}\mathbf{a}_{\mathrm{body}} \\ {}^{\mathrm{B}}\boldsymbol{\omega}_{\mathrm{body}} = {}^{\mathrm{B}}\mathbf{R}_{\mathrm{I}} \cdot {}^{\mathrm{I}}\boldsymbol{\omega}_{\mathrm{body}} \end{cases} \tag{2}$$

where, ${}^{\mathrm{B}}\mathbf{R}_{\mathrm{I}} \in \mathbb{R}^{3\times3}$ is the rotation matrix converted from the IMU frame {I} to the body frame {B}, which is determined by the posture of each section of the pipeline robot body and the installation position in the body frame {B}.

B. Estimation of the Body Attitude Angle of the Pipeline robot

The calculation method for the roll angle of the pipeline robot in the navigation frame {N} is given as:

$${}^{\mathrm{N}}\phi_{\mathrm{body}} = \arctan 2 \frac{{}^{\mathrm{N}}a_{\mathrm{y,body}}}{{}^{\mathrm{N}}a_{\mathrm{z,body}}} \tag{3}$$

where, $\arctan 2(\cdot)$ is the four quadrant arctangent function, ensuring an angle range of $[-\pi, \pi]$. ${}^{\mathrm{N}}a_{\mathrm{y,body}}$ and ${}^{\mathrm{N}}a_{\mathrm{z,body}}$ are the values measured by the accelerometer along the y-axis and z-axis in the navigation frame {N}, respectively.

Similarly, the calculation method for the pitch angle ${}^{\mathrm{N}}\theta_{\mathrm{body}}$ of the pipeline robot in the navigation frame {N} is expressed as:

$$ {}^{\mathrm{N}}\theta_{\mathrm{body}} = \arctan 2 \frac{-{}^{\mathrm{N}}a_{\mathrm{x,body}}}{\sqrt{{}^{\mathrm{N}}a_{\mathrm{y,body}}^2 + {}^{\mathrm{N}}a_{\mathrm{z,body}}^2}} \tag{4} $$

where, ${}^{\mathrm{N}}a_{\mathrm{x,body}}$ is the value measured by the accelerometer in the navigation frame {N}.

Under rough localization conditions, the approximate heading angle ${}^{\mathrm{N}}\psi_{body}^{\mathrm{int}}$ of the pipeline robot in the navigation frame {N} can be obtained by integrating the gyroscope angular velocity as follows:

$$ {}^{\mathrm{N}}\psi_{\mathrm{body}}^{\mathrm{int}}(k) = {}^{\mathrm{N}}\psi_{\mathrm{body}}^{\mathrm{int}}(k\text{-}1) + {}^{\mathrm{N}}\omega_{\mathrm{z,body}}(k)\cdot\Delta t \tag{5} $$

where, ${}^{\mathrm{B}}\omega_{\mathrm{z,body}}(k)$ is the angular velocity of the robot's body around the z-axis in the navigation frame {N} at time step k, and ${}^{\mathrm{B}}\psi_{\mathrm{body}}^{\mathrm{int}}(k)$ is the heading angle of the robot's body in the navigation frame {N} at time step k. However, since the cumulative error of angular velocity will affect the accuracy of the heading angle calculation [18], it is necessary to combine with the magnetometer for calibration. The expression for the calibrated heading angle is

$$ {}^{\mathrm{B}}\psi_{\mathrm{body}}^{\mathrm{adj}}(k) = F\left({}^{\mathrm{N}}\phi_{\mathrm{body}}, {}^{\mathrm{N}}\theta_{\mathrm{body}}, {}^{\mathrm{N}}\psi_{\mathrm{body}}^{\mathrm{int}}\right) \tag{6} $$

where， $\mathrm{F}(\cdot)$ is the magnetometer calibration function.

C. Wheel Odometer

The pipeline robot has three pairs of roll wheels, each of which is rigidly connected through a rolling shaft in the middle, and each roll wheel is transmitted to the motor through a bevel gear. Therefore, if the wheels do not slip, the distance s_{robot} that the robot advances can be calculated based on the pulse increments of the motors,

$$ s_{\mathrm{body}} = \frac{\left(n_{\mathrm{pulse},1} + n_{\mathrm{pulse},2} + n_{\mathrm{pulse},3}\right)}{3\cdot \mathrm{m}_{\mathrm{pulse}}} \cdot \pi \cdot \mathrm{d}_{\mathrm{wheel}} \tag{7} $$

where, $\mathrm{m}_{\mathrm{pulse}}$ is the number of pulses per rotation of the motor, and $\mathrm{d}_{\mathrm{wheel}}$ denotes the diameter of the roll wheel. $n_{\mathrm{pulse},1}$, $n_{\mathrm{pulse},2}$, and $n_{\mathrm{pulse},3}$ are the pulse increments of the three motors that drive each roll wheel respectively. By differentiating the equation (7) over time, the speed of the robot v_{body} can be obtained as follows:

$$ v_{\mathrm{body}} = \frac{\Delta s_{\mathrm{body}}}{\Delta \mathrm{t}} \tag{8} $$

D. Dead Reckoning Calculation

The EKF method can be used to optimize the attitude angle estimation [18]. Firstly, the state equation and observation equation of the body attitude angle on the navigation frame {N} can be established. The sampling time is Δt , and the state vector is given as

$$ \mathbf{X}_k = [{}^{\mathrm{N}}\phi_{\mathrm{body}}(k), {}^{\mathrm{N}}\theta_{\mathrm{body}}(k), {}^{\mathrm{N}}\psi_{\mathrm{body}}(k)]^{\mathrm{T}} \tag{9} $$

using the Euler angle method, the state equation of the system is set as:

$$ \mathbf{X}_k = \mathrm{A}(\mathbf{X}_{k\text{-}1}) + \mathbf{W}_k \tag{10} $$

where, $\mathrm{A}(\cdot)$ is the state transition function, and $\mathbf{W}_{kI} \in \mathbb{R}^{3\times 1}$ is the process noise vector. The observation of attitude angle can be jointly calculated by accelerometer and magnetometer, and the observation vector is:

$$ \mathbf{Z}_{\mathrm{k}} = [{}^{\mathrm{N}}\phi_{\mathrm{body}}^{\mathrm{obs}}(k), {}^{\mathrm{N}}\theta_{\mathrm{body}}^{\mathrm{obs}}(k), {}^{\mathrm{N}}\psi_{\mathrm{body}}^{\mathrm{obs}}(k)]^{\mathrm{T}} \tag{11} $$

The observation equation is：

$$ \mathbf{Z}_{\mathrm{k}} = \mathrm{H}(\mathbf{X}_{\mathrm{k}}) + \mathbf{V}_k \tag{12} $$

where, $\mathrm{H}(\cdot)$ is the state observation function, and $\mathbf{V}_k \in \mathbb{R}^{3\times 1}$ is the observation noise vector. To linearize, expand the Taylor series of the system's state equation and take a first-order approximation. The linearized expression is:

$$ \mathbf{L}_{\mathrm{k,k\text{-}1}} = \left.\frac{\partial \mathrm{A}(\mathbf{X})}{\partial(\mathbf{X})}\right|_{\mathbf{X}=\hat{\mathbf{X}}_{\mathrm{k,k\text{-}1}}} \tag{13} $$

applying the above approximate linearization model to the basic process of discrete Kalman filtering is given as follows [18]:

$$ \begin{cases} \mathbf{X}_{k/k\text{-}1} = \mathbf{L}_{k,k\text{-}1}\cdot\mathbf{X}_{k\text{-}1} \\ \mathbf{P}_{k/k\text{-}1} = \mathbf{L}_{k,k\text{-}1}\cdot\mathbf{P}_{k\text{-}1}\cdot\mathbf{L}_{k,k\text{-}1}^{\mathrm{T}} + \mathbf{G}_{k\text{-}1}\cdot\mathbf{Q}_{k\text{-}1}\cdot\mathbf{G}_{k\text{-}1}^{\mathrm{T}} \\ \mathbf{K}_k = \mathbf{P}_{k/k\text{-}1}\cdot\mathbf{H}_k^{\mathrm{T}}(\mathbf{H}_k\cdot\mathbf{P}_{k/k\text{-}1}\cdot\mathbf{H}_k^{\mathrm{T}} + \mathbf{R}_k)^{\text{-}1} \\ \mathbf{X}_k = \mathbf{X}_{k/k\text{-}1} + \mathbf{K}_k\cdot(\mathbf{Z}_k - \mathbf{H}_k\cdot\mathbf{X}_{k/k\text{-}1}) \\ \mathbf{P}_k = (\mathrm{I}\text{-}\mathbf{K}_k\cdot\mathbf{H}_k)\cdot\mathbf{P}_{k/k\text{-}1} \end{cases} \tag{14} $$

where, $\mathbf{X}_{k/k\text{-}1} \in \mathbb{R}^{3\times 1}$ denotes the a priori predicted state estimate at time step k, derived by applying the state transition matrix $\mathbf{L}_{k,k\text{-}1} \in \mathbb{R}^{3\times 3}$ to the a posteriori updated state estimate from $\mathbf{X}_{k\text{-}1} \in \mathbb{R}^{3\times 1}$ the previous time step k-1. $\mathbf{P}_{k/k\text{-}1} \in \mathbb{R}^{3\times 3}$ is the priori covariance matrix of the state estimate at time step k, which is computed by transforming the a posteriori covariance matrix $\mathbf{P}_{k\text{-}1} \in \mathbb{R}^{3\times 3}$ from time step k-1 using $\mathbf{L}_{k,k\text{-}1}$, plus a term involving the process noise input matrix $\mathbf{G}_{k\text{-}1} \in \mathbb{R}^{3\times 3}$ and the process noise covariance matrix $\mathbf{Q}_{k\text{-}1} \in \mathbb{R}^{3\times 3}$. $\mathbf{K}_k \in \mathbb{R}^{3\times 3}$ represents the Kalman gain at time step k, balancing the trade-off between the predicted state and the new observation. It is

calculated using $\mathbf{P}_{k/k\text{-}1}$, the observation matrix $\mathbf{H}_k \in \mathbb{R}^{3\times3}$, and the observation noise covariance matrix $\mathbf{R}_k \in \mathbb{R}^{3\times1}$. $\mathbf{X}_k \in \mathbb{R}^{3\times1}$ is the posteriori updated state estimate at time step k, refined by correcting $\mathbf{X}_{k/k\text{-}1}$ with the Kalman gain $\mathbf{K}_k$ applied to the observation residual $(\mathbf{Z}_k - \mathbf{H}_k \cdot \mathbf{X}_{k/k\text{-}1})$, where $\mathbf{Z}_k \in \mathbb{R}^{3\times1}$ is the observation at time step k and $\mathbf{H}_k$ maps the state to the observation space. Lastly, $\mathbf{P}_k \in \mathbb{R}^{3\times1}$ is the posteriori covariance matrix of the state estimate at time step k, describing the uncertainty in the updated state, which can be obtained by transforming $\mathbf{P}_{k/k\text{-}1}$ with the term $(\mathrm{I}\text{-}\mathbf{K}_k \cdot \mathbf{H}_k)$, where I is the identity matrix.

Based on the body attitude angles obtained from the EKF measurements above, the position coordinate ${}^{\mathrm{N}}\mathbf{P}_{\mathrm{body}}(k) \in \mathbb{R}^{3\times1}$ of the pipeline robot at the time step k in the navigation frame {N} can be calculated as follows:

$$\begin{cases} {}^{\mathrm{N}}x(k) = {}^{\mathrm{N}}x(k-1) + {}^{\mathrm{N}}v_{\mathrm{body}}(k)\cdot\Delta t\cdot\cos\left({}^{\mathrm{N}}\theta_{\mathrm{body}}^{\mathrm{EKF}}(k)\right)\cdot\cos\left({}^{\mathrm{N}}\psi_{\mathrm{body}}^{\mathrm{EKF}}(k)\right) \\ {}^{\mathrm{N}}y(k) = {}^{\mathrm{N}}y(k-1) + {}^{\mathrm{N}}v_{\mathrm{body}}(k)\cdot\Delta t\cdot\cos\left({}^{\mathrm{N}}\theta_{\mathrm{body}}^{\mathrm{EKF}}(k)\right)\cdot\sin\left({}^{\mathrm{N}}\psi_{\mathrm{body}}^{\mathrm{EKF}}(k)\right) \\ {}^{\mathrm{N}}z(k) = {}^{\mathrm{N}}z(k-1) + {}^{\mathrm{N}}v_{\mathrm{body}}(k)\cdot\Delta t\cdot\sin\left({}^{\mathrm{N}}\theta_{\mathrm{body}}^{\mathrm{EKF}}(k)\right) \end{cases} \quad (15)$$

where, ${}^{\mathrm{N}}\theta_{\mathrm{body}}^{\mathrm{EKF}}(k)$ and ${}^{\mathrm{N}}\psi_{\mathrm{body}}^{\mathrm{EKF}}(k)$ are the body pitch and yaw angles estimated by EKF algorithm at the time step k in the navigation frame {N}, respectively. By acquiring the absolute position of the robot in the world frame {W} at all motion moments, the positioning trajectory of the pipeline can be derived:

$${}^{\mathrm{W}}\mathbf{P}_{\mathrm{robot}}(k) = {}^{\mathrm{W}}\mathbf{P}_{\mathrm{start}} + {}^{\mathrm{W}}\mathbf{R}_{\mathrm{N}} \cdot {}^{\mathrm{N}}\mathbf{P}_{\mathrm{robot}}(k) \quad (16)$$

where, ${}^{\mathrm{W}}\mathbf{R}_{\mathrm{N}} \in \mathbb{R}^{3\times1}$ is the rotation transformation matrix between the navigation frame {N} and the world frame {W} at the start of motion. ${}^{\mathrm{W}}\mathbf{P}_{\mathrm{start}} \in \mathbb{R}^{3\times1}$ denotes the absolute position coordinates of the pipeline robot in the world frame {W} at the start of motion, which is obtained via Real-Time Kinematic (RTK) positioning technology.

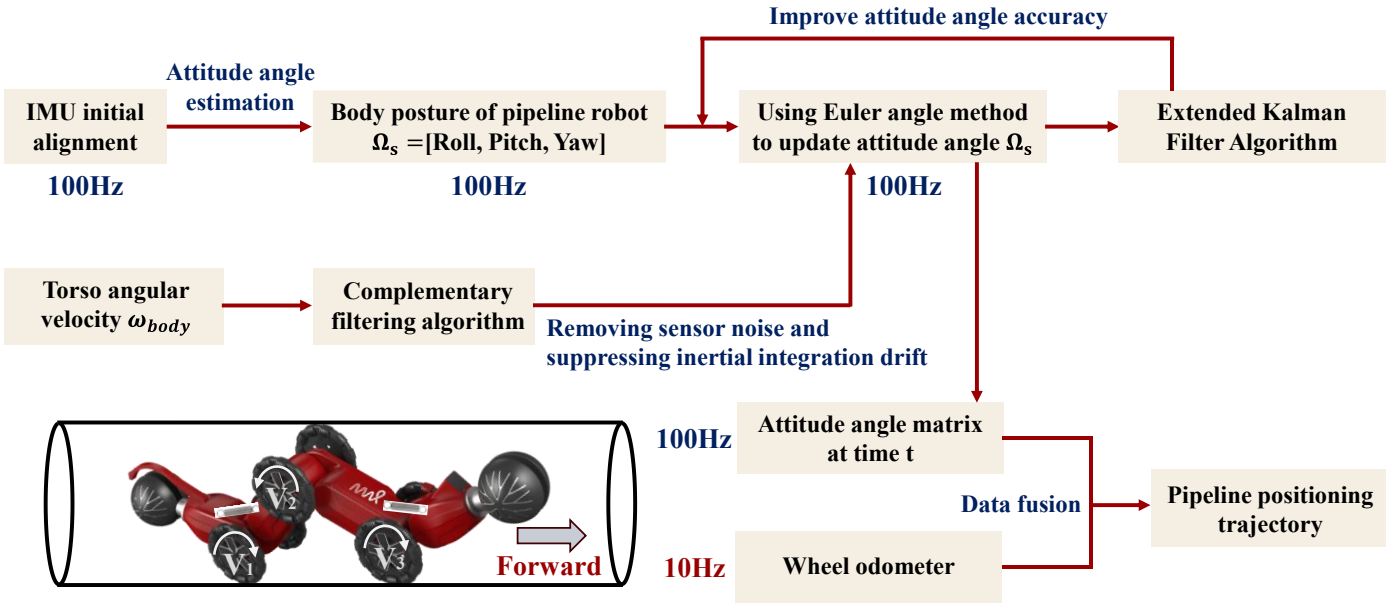

Fig. 4. Schematic diagram of dead reckoning algorithm method for pipeline robots in complex pipeline networks.

Fig. 4 presents our schematic diagram of dead reckoning algorithm method for pipeline robots in complex pipeline networks. First, the IMU is initially aligned, and the alignment result is input to the 100Hz body angle estimation module. Simultaneously, the robot's torso angular velocity is processed by a complementary filtering algorithm to remove sensor noise and suppress inertial integral drift. Then, the robot's body attitude angles and the filtered angular velocity data are input into the attitude angle update process based on the Euler angle method to refresh the attitude. Subsequently, the updated attitude angles are further optimized using an EKF algorithm to improve the attitude angle accuracy, obtaining the attitude angle matrix at the time t. Finally, the attitude angle data is fused with wheel odometry data, and the fusion result generates the robot's pipeline positioning trajectory.

IV. Experimental Verification and Result Analysis

A. Experiment Setting

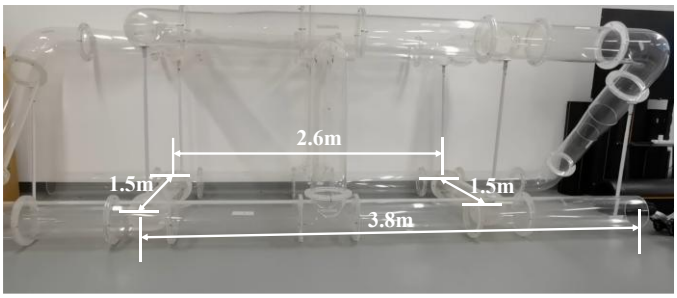

Fig. 5. Complex pipeline scene built in the laboratory using acrylic pipes.

As can be seen in Fig. 5, to verify the effectiveness of the proposed pipeline robot trajectory estimation method, we constructed an acrylic test pipeline scenario in the laboratory and conducted positioning tests using a rectangular loop at the bottom.

The pipeline robot has two control modes. The first is manual remote control, where motion control is achieved by sending commands via a remote controller. The robot rotates around the pipeline axis by rotating its front and rear ball wheels, while forward propulsion is provided by the frictional contact between three pairs of roll wheels and the pipe wall. The second is autonomous motion control. First, a connection is established between the laptop and the robot via a Wi-Fi hotspot. Then, the pre-written autonomous motion control program is uploaded to the upper-level motion control board (a quad-core ARM architecture, CPU 1.5GHz). The program is then executed to achieve automated motion. It is important to note that to ensure sufficient vertical pressure between the robot and the pipe wall, the stiffness of the robot's front and rear springs needs to be adjusted according to the actual test conditions: selecting springs with appropriate stiffness while ensuring smooth robot passage provides the necessary conditions for accurate trajectory estimation.

B. Experiment Results

As shown in Fig. 6, this is a positioning performance test of the pipeline robot in a complex pipeline. Its core objective is to achieve 3D positioning of the complex rectangular pipeline at the bottom. During the testing process, the entire movement time was approximately 161 seconds, and the robot's movement in a complex rectangular pipeline was recorded every 20 seconds. After entering the pipeline from the entrance, the robot completed a full circle along the rectangular pipeline and finally exited from the original entrance, successfully completing the complex rectangular pipeline crossing test.

Fig. 7 illustrates the velocity variation of the pipeline robot during pipeline trajectory positioning, with two curves corresponding to different velocity data. The orange dashed line represents the velocity curve directly calculated from the raw data of the wheel encoder, which shows obvious fluctuations due to sensor noise. In contrast, the blue solid line denotes the velocity after low-pass filtering, which can more clearly reflect the actual motion speed of the robot. The robot starts moving forward at approximately 4.1 seconds, then maintains a stable speed of about 0.069 m/s to perform pipeline trajectory positioning. When it reaches the turning section, the robot’s speed suddenly decreases. This adjustment is made to fine-tune the body posture, ensuring the robot can smoothly navigate into the bend without posture deviation. This velocity variation not only reflects the robot’s adaptive motion control in complex pipeline environments but also verifies that the low-pass filtering process effectively optimizes raw sensor data, providing reliable velocity input for subsequent positioning calculations.

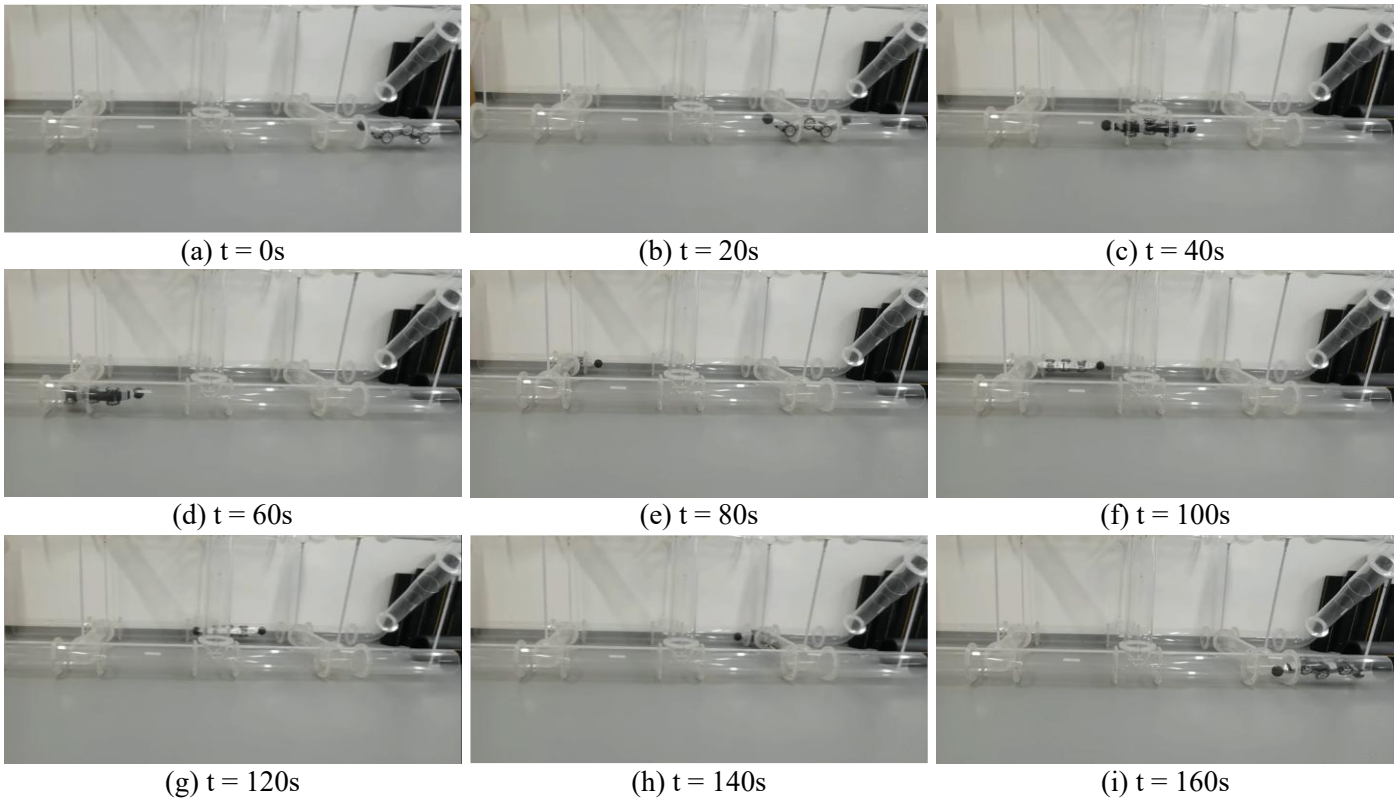

Fig. 6. Pipeline robots perform positioning tests in complex pipelines and draw three-dimensional trajectories of complex rectangular pipelines at the bottom.

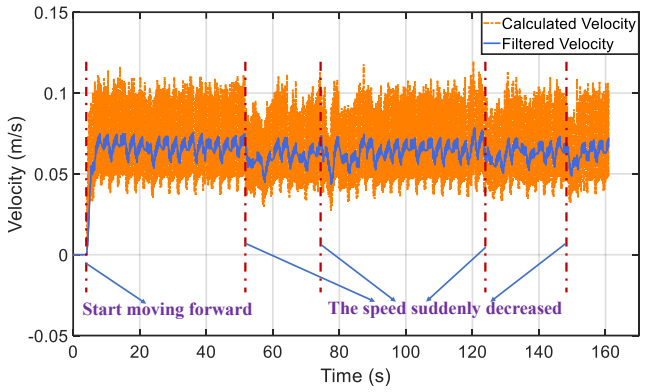

Fig. 7. The speed variation of pipeline robots in complex pipeline trajectory positioning.

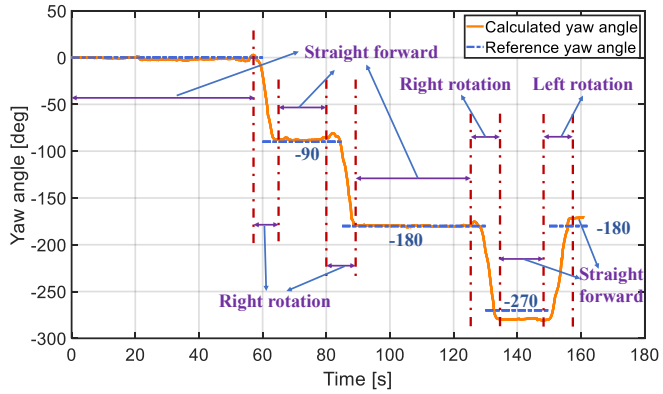

Fig. 8. The variation of heading angle of pipeline robot in complex pipeline trajectory positioning.

Fig. 8 shows the variation of the heading angle of the pipeline robot when operating in a complex pipeline environment. After entering the rectangular pipeline, the robot adjusts its body posture to navigate the layout. The robot performs three right rotations while passing through successive three-way pipelines, then makes a left rotation at the final three-way pipeline before returning to its starting position. In the local navigation frame {N}, the initial heading angle is set to 0 degrees. The orange solid line in the figure represents the heading angle calculated via the proposed trajectory estimation method, while the blue dotted line denotes the actual heading angle that aligns with the rectangular pipeline's structural layout. As reflected in the plot, the robot's body heading angle changes significantly during cornering segments to adapt to the pipeline's turns, whereas it remains nearly stable when moving along straight sections. This close alignment between the calculated heading angle (the orange solid line) and the actual heading angle (the blue dotted line) matches both the sharp variations in turns and minimal changes in straight segments, and directly verifies the effectiveness of the dead reckoning algorithm for the self-propelled pipeline robot proposed in this article.

As can be seen in Fig. 9, the orange solid line represents the trajectory estimated by the proposed algorithm while the blue dotted line denotes the actual trajectory of the pipeline in the test scenario. The experiment was conducted in a rectangular pipeline with a length of 2.6 meters and a width of 1.5 meters. When the robot passed through the third bend, the proposed dead reckoning algorithm resulted in a deviation of 0.13 meters along the X-axis and 0.23 meters along the Y-axis. When the robot returned to its starting position, the deviation in the Y-axis direction was 0.3m, achieving a positioning accuracy of about 1/10. The positioning deviation is attributed to the modular assembly of the self-propelled pipeline robot. Although the posture between each module can be adjusted, the installed inertial navigation unit's position is affected by changes in the robot's body posture, which in turn impacts positioning accuracy.

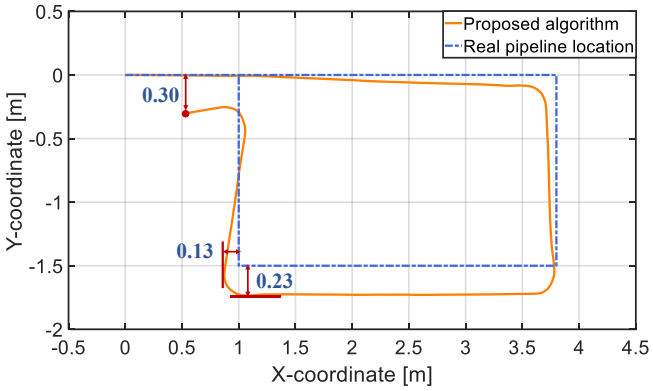

Fig. 9. Localization results of pipeline robots in complex pipelines.

V. Conclusion

This paper introduces a dead reckoning algorithm for a self-propelled pipeline robot in three-dimensional complex and confined pipeline environments, and verifies the effectiveness of the method through experiments using a self-developed robot prototype. By integrating an IMU module into the pipeline robot and utilizing its excellent mobility, wireless communication, and self-powering capabilities, the pipeline robot overcomes the limitations of traditional cables, enabling self-localization and pipeline trajectory mapping within complex pipelines. The proposed dead reckoning algorithm first acquires the robot's attitude angles using the IMU, then optimizes the attitude angle estimation accuracy using the EKF algorithm, and finally fuses wheel odometry data to achieve high-precision pipeline positioning. However, there may be impurities such as water and coal ash inside the real gas pipeline, which can cause tire slippage. The drift caused by the long-term operation of the inertial navigation system can also affect the positioning accuracy.

Our future work will focus on researching positioning algorithm optimization and dynamic error compensation technology to further improve the robustness of dead reckoning algorithm in long-distance, high-interference pipeline environments. In addition, our ultimate goal is to achieve autonomous motion control and routine inspection of pipeline robots in gas pipelines.

Acknowledgment

Thanks to the researchers of DeepCavas (Beijing) Technology Co., Ltd. for their support and assistance during the experimental implementation.

References

[1] Q. Xiao, J. Li, J. Sun, et al., "Natural-gas pipeline leak location using variational mode decomposition analysis and cross-time–frequency spectrum," *Measurement*, vol. 124, pp. 163–172, 2018.

[2] H. Li, C. Chou, L. Fan, et al., "Toward automatic subsurface pipeline mapping by fusing a ground-penetrating radar and a camera," *IEEE Trans. Autom. Sci. Eng.*, vol. 17, no. 2, pp. 722–734, 2019.

[3] G. Bernasconi and G. Giunta, "Acoustic detection and tracking of a pipeline inspection gauge," *J. Pet. Sci. Eng.*, vol. 194, p. 107549, 2020.

[4] R. He, Y. Guo, L. Sun, et al., "Investigation of the position detection approach for deeply buried steel pipelines based on the electromagnetic method," *Meas. Sci. Technol.*, vol. 36, no. 10, p. 105011, 2025.

[5] S. Du, H. Zhang, C. Gong, et al., "A Pipeline Inspection Gauge Positioning Method Based on Distributed Fiber Optic Vibration Sensing," *IEEE Sens. J.*, 2024.

[6] O. Álvarez-Tuñón, Y. Brodskiy, E. Kayacan, "Monocular visual simultaneous localization and mapping: (r)evolution from geometry to deep learning-based pipelines," *IEEE Trans. Artif. Intell.*, vol. 5, no. 5, pp. 1990–2010, 2023.

[7] S. Karam, M. Peter, S. Hosseinyalamdary, et al., "An evaluation pipeline for indoor laser scanning point clouds," *ISPRS Annals Photogramm*. Remote Sens. Spatial Inf. Sci., vol. 4, pp. 85–92, 2018.

[8] X. Zhou, Q. Chen, B. Jiang, et al., "An underground pipeline mapping method based on fusion of multisource data," *IEEE Trans. Geosci. Remote Sens.*, vol. 60, pp. 1–11, 2022.

[9] Q. Chen, Q. Zhang, X. Niu, et al., "Positioning accuracy of a pipeline surveying system based on MEMS IMU and odometer: Case study," *IEEE Access*, vol. 7, pp. 104453–104461, 2019.

[10] A. Kakogawa, C. Hirose, and S. Ma, "A standards-based pipeline route drawing system using a towed sensing unit," *in Proc. IEEE/RSJ Int. Conf. Intell. Robots Syst. (IROS)*, Kyoto, Japan, *2022,* pp. 7167–7173.

[11] A. Kakogawa, K. Murata, and S. Ma, "Automatic t-branch travel of an articulated wheeled in-pipe inspection robot using joint angle response to environmental changes," *IEEE Trans. Ind. Electron.*, vol. 70, no. 7, pp. 7041–7050, Jul. 2023.

[12] R. Konishi, M. Nakajima, K. Tanaka, et al., "Design for snake robot motion via partial grasping on pipes," *Adv. Robot.*, vol. 37, no. 4, pp. 227–240, 2023.

[13] S. Roh and H. R. Choi, "Differential-drive in-pipe robot for moving inside urban gas pipelines," *IEEE Trans. Robot.*, vol. 21, no. 1, pp. 1–17, 2005.

[14] H. M. Kim, Y. S. Choi, Y. G. Lee, et al., "Novel mechanism for in-pipe robot based on a multiaxial differential gear mechanism," *IEEE/ASME Trans. Mechatron.*, vol. 22, no. 1, pp. 227–235, 2016.

[15] Y. Wu, J. Kuang, and X. Niu, "Wheel-INS2: Multiple MEMS IMU-based dead reckoning system with different configurations for wheeled robots," *IEEE Trans. Intell. Transp. Syst.*, vol. 24, no. 3, pp. 3064–3077, 2022.

[16] J. Wang, Z. Pan, Z. Niu, et al., "Estimation of ground posture angle for quadruped robots based on IMU," in *Proc. 2023 6th Int. Conf. Electron. Technol. (ICET), IEEE*, 2023, pp. 1269–1275..

[17] W. Wang, D. Yang, J. Zhang, et al., "A dead reckoning localization method for in-pipe detector of water supply pipeline: An application to leak localization," *Measurement*, vol. 171, p. 108835, 2021.

[18] E. H. Shin and N. El-Sheimy, "Navigation Kalman filter design for pipeline pigging," *J. Navig.*, vol. 58, no. 2, pp. 283–295, 2005.